Limnol. Oceanogr., 51(6), 2006, 2646–2659

Red and black tides: Quantitative analysis of water-leaving radiance and perceived color for phytoplankton, colored dissolved organic matter, and suspended sediments

Heidi M. Dierssen[1]
Department of Marine Science, University of Connecticut, 1080 Shennecossett Road, Groton, Connecticut 06340

Raphael M. Kudela
Ocean Sciences Department, University of California, Santa Cruz, California 95064

John P. Ryan
Monterey Bay Aquarium Research Institute, 7700 Sandholdt Road, Moss Landing, California 95039

Richard C. Zimmerman
Department of Ocean, Earth, and Atmospheric Sciences, 4600 Elkhorn Avenue, Old Dominion University, Norfolk, Virginia 23529

Abstract

Using field measurements and quantitative modeling, we demonstrate that red coloration of the sea surface is not associated with any particular group of phytoplankton and is strongly dependent on the physiology of the human visual system. Red or brown surface waters can be produced by high concentrations of most types of algae, colored dissolved organic matter, or suspended sediment. Even though light reflected by red tides commonly peaks in the yellow spectral region (570–580 nm), human color perception requires consideration of the entire spectrum of light relative to receptors within the human eye. The color shift from green to red is not due to any special optical properties of the algae but results from an overlap in spectral response of the eye's red and green cones (centered at 564 and 534 nm, respectively). The spectral peak in light reflected from dense algal blooms coincides with a critical hinge point in color vision (570–580 nm), where fine-scale shifts in the spectral shape of water-leaving radiance due to algal absorption and backscattering properties lead to pronounced variations in the observed color. Of the taxa considered, only Chlorophytes and Prochlorophytes lacked sufficient accessory pigments to produce a red tide. Chlorophyll fluorescence and enhanced near-infrared reflectance (the "red edge") contribute negligibly to the perceived color. Black water events are produced when water is highly absorbing but lacks backscattering constituents.

The first of the 10 plagues of Egypt may be one of the earliest recorded instances of a red tide: "and all the waters that were in the river turned to blood. And the fish that were in the river died, and the water stank" (The Bible, Exodus 7:20–21). Red tides have been known to occur throughout human history; however, human activities and population increases have contributed to a greater abundance of toxic and noxious algal blooms in coastal regions worldwide (Hallegraeff 2003; Glibert et al. 2005). Dense algal blooms are often called red tides because the sea surface becomes discolored red or ruddy brown. In addition, red tide is often used synonymously with harmful algal blooms (HAB), the term used by the scientific community to characterize all plankton events that have deleterious impacts. However, not all algal blooms that produce red or brown colored water are toxic. Conversely, not all harmful algal blooms are associated with red-colored waters (Anderson 1994), nor are they tidally driven. Despite these discrepancies, the term red tide has been widely adopted by the popular media and is commonly used to refer to intense algal blooms worldwide.

Water color has long been used to define water masses since the introduction of the Forel-Ule color scale in the late 1800s (Hutchinson 1975; Arnone et al. 2004). Color No. 21 on this scale has a reddish-brown hue that could be associated with a red tide event. However, the reason for red coloration of intense algal blooms is often misunderstood. The Encyclopedia Britannica (2004) describes red tides as "a discoloration of sea water caused by dinoflagellates (phylum Protozoa) during periodic blooms (or population increases)." The underlying assumption is that red tide–forming phytoplankton contain a unique suite of

[1] Corresponding author (heidi.dierssen@uconn.edu).

Acknowledgments

We thank Dariusz Stramski for generously providing phytoplankton absorption and scattering spectra and Grace Chang for permission to use her spectrum and photograph of a natural red tide. Collin Roesler and the anonymous reviewers provided numerous helpful comments that greatly improved this manuscript.

Funding was provided by the David and Lucile Packard Foundation, NASA Ocean Biology and Biogeochemistry, Office of Naval Research Environmental Optics, and the NOAA Coastal Technology System (COTS, http://www.csc.noaa.gov/cots) under a partnership with the Center for Integrated Coastal Observation, Research and Education (CICORE) and Center for Integrated Marine Technology (CIMT).

light-absorbing pigments that make them reddish in color. However, absorption properties of red tide–forming phytoplankton are not generally unique from other phytoplankton, and hence reddish pigments cannot solely be responsible for the color of red tides (Millie et al. 1997; Schofield et al. 1999; Roesler et al. 2003). In addition to pigmentation, algal scattering, particularly backscattering, is influenced by the cell size and potential growth phase of the phytoplankton (McLeroy-Etheridge and Roesler unpubl. data) and is an important optical property determining the magnitude and spectral shape of the emergent light field.

A comprehensive analysis of the optics of red tides has been hampered by the use of radiometers incapable of fully resolving the visible spectrum (i.e., from 400 to 700 nm). Most in-water optical sensors launched over the last few decades measure light in only six or seven visible channels that match those measured from most space-borne ocean color sensors (Yoder 2000). These channels are not evenly spaced throughout the visible spectrum and are concentrated in blue and green wavelengths between 412 and 555 nm. Consequently, a large spectral gap occurs between the green channel at 555 nm and the red channel around 665 nm. Light reflected from red tides commonly peaks from 570–580 nm, a part of the visible spectrum that is not generally quantified by these multispectral sensors. Moreover, the region between 555 and 665 nm is critical for accurately modeling the color perceived by the human eye. The development of a new class of hyperspectral sensors that provide continuous spectral coverage over the entire visible spectrum (Chang et al. 2004) has allowed us to quantify the spectrum of light incident upon the human eye.

Following on past research (Morel and Prieur 1977; Carder and Steward 1985; Roesler et al. 2003), we use radiative transfer modeling to estimate the water-leaving radiance from sea surface expressions of different concentrations and types of phytoplankton, colored dissolved organic matter (CDOM), and minerals. The color of the water perceived by a human eye is estimated for each spectrum using the color matching functions defined by the Commission Internationale de l'Êclairage (CIE 1991). The perceived color assumes that the individual is looking directly down at a relatively calm sea surface with no contrasting skylight or sea surface glint. Color shifts from blue to green to brown and red can be quantitatively modeled from typical absorption and backscattering properties of phytoplankton, CDOM, and/or minerals.

Methods

Phytoplankton absorption and chlorophyll—Absorption coefficients for particulate material were determined using a Cary 50 dual-beam spectrophotometer. Water samples (25 mL) were filtered onto Whatman GF/F filters. Phytoplankton (a_{ph}) spectra were determined by subtraction of detrital absorption (Tassan and Ferrari 1995) from particulate absorption and correction for multiple scattering caused by the filter material (Cleveland and Weidemann 1993). Published absorption spectra were also used (Stramski et al. 2001). Phytoplankton absorption coefficients were normalized to the corresponding chlorophyll *a* (Chl *a*) concentration. Chl *a* was determined fluorometrically by filtration onto Whatman GF/F filters and extraction in acetone at -20°C for 24–48 h (Smith et al. 1981) using pure Chl *a* (Sigma) as a calibration reference.

Hyperspectral reflectance measurements—Two different field methods were employed to measure remote sensing reflectance, R_{rs}, defined as water-leaving radiance, L_w, normalized to incident irradiance. In-water measurements were made with hyperspectral radiometers, Hyperspectral Tethered Spectroradiometer Buoy (HTSRB, Satantic, Inc.) and HyperPro II (Satlantic Inc.). The radiative transfer model, *Hydrolight*, was parameterized with coincident *ac*-9 measurements (WET Labs) and relevant ancillary data (e.g., latitude, longitude, day of the year, time) to develop site-specific spectral coefficients from the ratio of modeled water-leaving radiance and radiance modeled at the depth of the upwelling radiance sensors of the HTSRB and HyperPro radiometers (0.6 and 0.2 m, respectively). These coefficients were applied to the original hyperspectral upwelling radiance measurements to correct for absorption and scattering processes in the upper layer of water and extrapolate values across the air–sea interface. Above-surface radiances were measured with a Field Spec Pro VNIR-NIR1 portable spectrometer system (Analytical Spectral Devices) along Monterey Bay and the California coast in conjunction with Center for Integrative Coastal Observation, Research, and Education (CICORE), California State University. Measurements were made with an 8° foreoptic focused at a $40–45^{\circ}$ angle sequentially on a gray plaque, sea surface, and diffuse sky. Residual reflected sky radiance was removed from the calculated R_{rs} assuming that the mean reflectance from 750–800 nm was zero (Mobley 1999).

Reflectance of dense cultures of phytoplankton taxa was also measured in the laboratory using the Field Spec Pro VNIR-NIR1 portable spectrometer system (Analytical Spectral Devices) and integrating sphere attachment calibrated for baseline reflectance using a Spectralon plaque. Dense, log-phase cultures of the microalgae *Thalassiosira* sp., *Coccolithophora* sp., *Porphyridium* sp., and *Amphidinium* sp. were obtained from Wards Natural Science, Inc. Cells were captured onto Whatman GF/F filters using a gentle vacuum and immediately placed into the reflectance port of the integrating sphere. These measurements are relative reflectance spectra and have not been corrected for filter effects (Balch and Kilpatrick 1992).

Modeling water-leaving radiance—The radiative transfer model *Hydrolight* was employed to estimate the radiance leaving the water column composed of varying amounts of phytoplankton (Mobley 1994). Water-leaving radiance, L_w, was modeled assuming dense accumulations of algae at the sea surface (2–50 mg Chl *a* m^{-3}). Optical variability due to depth-dependent layers of algae was not considered here. Inputs to the model included: taxon-specific chlorophyll-

normalized absorption (*see Methods*), chlorophyll-specific scattering coefficients (Stramski et al. 2001), and a semi-empirical sky model with a solar zenith angle of 55°, wind speed of 5 m s^{-1}, and an infinitely deep water column that included Raman scattering and chlorophyll fluorescence (Mobley 1994). For the average case, a Fournier-Forand particle phase function (Fournier and Forand 1994) was used with a particulate backscattering ratio of 0.012 (Ulloa et al. 1994). This is within the range of backscattering ratios found in oceanic waters throughout the world (Twardowski et al. 2001; Sullivan et al. 2005) and was found to be an average value for achieving optical closure with *Hydrolight* in coastal waters sampled in conjunction with the CICORE program (0.7 to 50 mg Chl *a* m^{-3}). In the sensitivity analysis, the particulate backscattering ratio varied from 0.006 to 0.02. For the phytoplankton simulations, CDOM was set to be proportional to Chl *a* at 440 nm (Mobley 1994), although this is not necessarily the case in more optically complex waters. The absorption by CDOM in all simulations was much lower than either the absorption by phytoplankton or that needed to induce a red tide from CDOM alone (*see following*).

Hydrolight was also used to estimate water-leaving radiance due to increasing amounts of CDOM and minerals, respectively. A single exponential CDOM model was used with a spectral slope of 0.015 (Twardowski et al. 2004) and soluble absorption coefficients, a_g^* (412), ranging from 0.1 to 15 m^{-1}. The model was also run with increasing amounts of four different types of minerals: brown earth, red clay, yellow clay, and calcareous sand. Mass-specific absorption and scattering coefficients were obtained from Ahn (1990), as supplied with the *Hydrolight* model (Mobley 1994). The absorption coefficients fall within the range of recent measurements from a variety of mineral particles (Babin and Stramski 2004). A Fournier-Forand particle phase function of 0.025 was used for the mineral simulations (Fournier and Forand 1994; Twardowski et al. 2001; Sullivan et al. 2005).

Color modeling—The Commission Internationale de l'Êclairage (CIE) developed a universally recognized objective system of colorimetry whereby the spectral distribution of light can be used to derive *Y*, the luminance or brightness, and two chromaticity parameters, *x* and *y*, representing the hue and saturation (Williamson and Cummins 1983). This system is based on color matching functions (tristimulus functions) that have been derived for the average human subject and are considered to be reasonably accurate and reproducible. However, the apparent color is not only a function of the light that falls on the localized region of the retina, but can also depend on the surrounding field or background colors. Contrast phenomena that can alter the apparent color (e.g., bright sky vs. dark water) are not considered here. We assume the human observer is looking directly down at the sea surface with no sun glint or bright sky for contrast.

The water-leaving radiance spectra were converted into color using the three tristimulus functions for a 10° field of view ($\bar{x},\bar{y},\bar{z}$) (CIE 1991). The CIE color components were estimated as the products of the radiance spectrum and three tristimulus functions integrated over the visible spectrum (400–700 nm), such that

$$X = K_m \int_{400}^{700} L_w(\lambda)\bar{x}(\lambda)d\lambda \quad (1)$$

$$Y = K_m \int_{400}^{700} L_w(\lambda)\bar{y}(\lambda)d\lambda \quad (2)$$

$$Z = K_m \int_{400}^{700} L_w(\lambda)\bar{z}(\lambda)d\lambda \quad (3)$$

In calculation of the CIE chromaticity coordinates (*x, y*), the conversion factor K_m cancels out of the equation and

$$(x,y) = \left(\frac{X}{(X + Y + Z)}, \frac{Y}{(X + Y + Z)}\right) \quad (4)$$

However, the magnitude of K_m is important for determining the perceived brightness or luminance of a spectrum and for converting from CIE coordinates into computer-based red–green–blue (RGB) coordinates. To determine whether the radiance spectrum is too low for human vision and the water appears dark or black, K_m is set to the maximum luminous efficacy for photopic (daylight) vision of 638 lumen (lm) W^{-1} (Mobley 1994). The water is determined to be black when the calculated luminance, *Y*, falls below 3 lm m^{-2} per steradian (sr^{-1}), which is the luminance for a twilight sky (Mobley 1994).

To determine the RGB color of a spectrum given its relative spectral shape, the conversion factor, K_m, must be normalized to the luminance, *Y*, where

$$K_m = \frac{0.4}{\int_{400}^{700} L_w(\lambda)\bar{y}(\lambda)d\lambda} \quad (5)$$

The empirical factor 0.4 produces colors in the midpoint of the brightness range for the RGB color system and adequately simulates seawater color. The CIE *X, Y*, and *Z* values are transformed into RGB primaries using a matrix transform based on the chromaticity coordinates and reference white of a standard computer monitor (ITU-R 2002), such that

$$\begin{bmatrix} R \\ G \\ B \end{bmatrix} = \begin{bmatrix} 3.240479 & -1.537150 & -0.498535 \\ -0.969256 & 1.875992 & 0.041556 \\ 0.055648 & -0.204043 & 1.057311 \end{bmatrix} \times \begin{bmatrix} X \\ Y \\ Z \end{bmatrix} \quad (6)$$

The resulting RGB coordinates range from 0 to 1 and represent the fractional amount of each primary needed to display a particular color on a computer monitor. Values calculated to be less than 0 were set to 0 and values greater

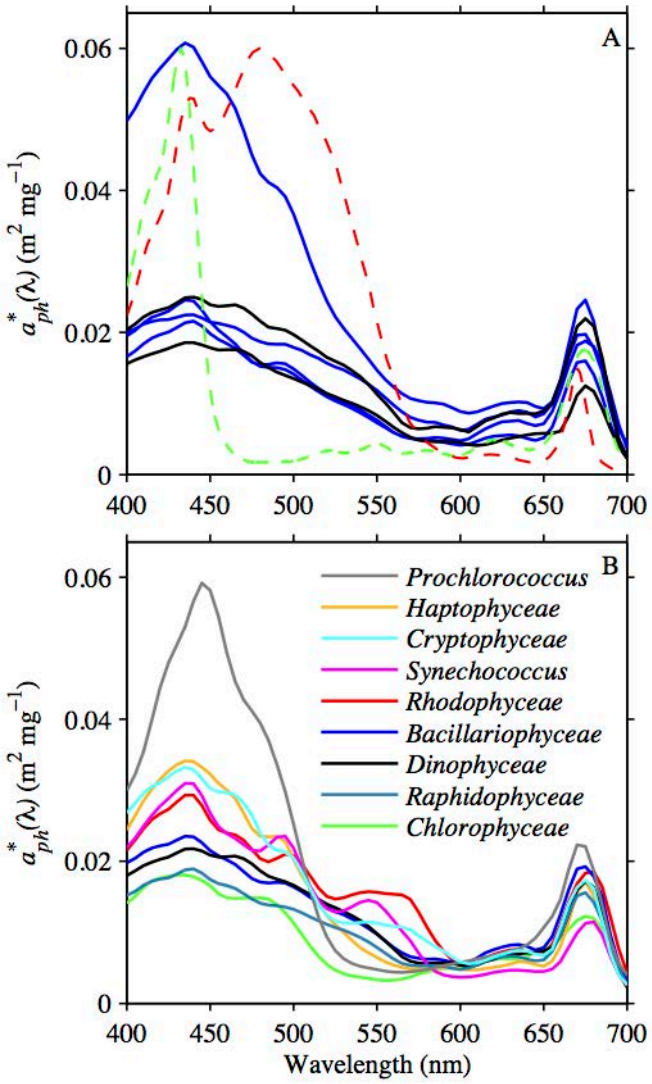

Fig. 1. (A) Absorption coefficient normalized to Chl *a*, a^*_{ph}, for different species of diatoms, Bacillariophyceae, and dinoflagellates, Dinophyceae. Green dashed line is an absorption spectrum for Chl *a* extracted in methanol and red dashed line is for the peridinin–chlorophyll–protein complex (scaled for figure) to illustrate the absorption due to accessory pigments. (B) Median absorption spectra normalized to Chl *a* for different phytoplankton communities (Stramski et al. 2001).

than 1 were set to 1. The MATLAB code for determining the RGB color of a spectrum is posted on the web (Dierssen 2006).

Results and discussion

The role of absorption—Phytoplankton contain pigments that absorb light of different wavelengths. Chlorophyll *a*, the dominant pigment found in all oxygenic photosynthetic organisms, absorbs light broadly in the Soret, or blue (400 to 470 nm), region and narrowly in the red (660 nm) part of the electromagnetic spectrum (Fig. 1A). The green color of most plants, therefore, is due to reflected green light that is not absorbed by Chl *a*. However, other accessory pigments found in phytoplankton—such as chlorophylls *b* and *c*, phycobiliproteins, and carotenoids—allow organisms to harvest more of the incident blue and green light. Phytoplankton from different taxa generally have unique sets of accessory pigments that differentiate them from one another (Sathyendranath et al. 1987; Cullen et al. 1997). Even so, the overall absorption spectra from many different phytoplankton taxa are generally not distinguishable (Fig. 1B). Larger phytoplankton tend to have lower absorption per mass of Chl *a* than smaller phytoplankton because of packaging of the pigments within the cells (Bricaud et al. 1995; Ciotti et al. 2002). As noted in Fig. 1B, small cells (e.g., Prochlorophytes) tend to have higher specific absorption than the larger cells (e.g., Bacillariophyceae or diatoms). Furthermore, algal absorption properties for each taxon will be influenced by the light environment in which it is grown (*see* Kirk 1994).

Dinoflagellates contain the carotenoid peridinin, which is considered to be reddish orange in color. The peridinin–chlorophyll–protein (PCP) complex broadens the blue absorption band from 470 to 555 nm (Fig. 1A). If peridinin were the cause of red tides, then the absorption spectrum for dinoflagellates containing peridinin should be significantly different from other phytoplankton taxa and should be shifted much further into the green region of the spectrum. However, absorption spectra from a variety of dinoflagellates are similar to other types of algae including diatoms, Bacillariophyceae (Fig. 1). Additionally, average absorption spectra from a variety of taxa show that most phytoplankton groups have accessory pigments that broaden the blue absorption band out to 550 nm (Stramski et al. 2001). Of the taxa considered, green algae (Chlorophyceae) absorb the least amount of green light, while red algae (Rhodophyceae) and *Synechococcus* absorb the most.

When observed under magnification, individual phytoplankton cells most frequently appear green, yellowish green, or golden in color and are generally not the ruddy color of red tides. Although accessory pigment concentrations can alter the color of individual cells enough to make them distinctly red or even violet, this is not a necessary condition for formation of a red tide. The color of individual cells does not necessarily represent the color of the cells when suspended in a solution or when highly concentrated. For example, yellow food coloring can appear orange or red at high concentrations. As quantified here, red tides can be formed from cells that are not themselves red.

The absorption spectra in Fig. 1 represent average conditions. Spectral deviations in absorption will be observed in response to environmental conditions, especially irradiance. Absorption could potentially also deviate from the normal when the cells are growing rapidly, as is required for an intense algal bloom. However, significant changes in the shapes of absorption spectra have not been observed for most harmful algal species measured during stationary and exponential growth phases (Harding 1998; McLeroy-Etheridge and Roesler unpubl. data). No special absorption properties appear to be associated with phytoplankton known to form red tides, and many different algal taxa have sufficient accessory pigments to produce red coloration when concentrated.

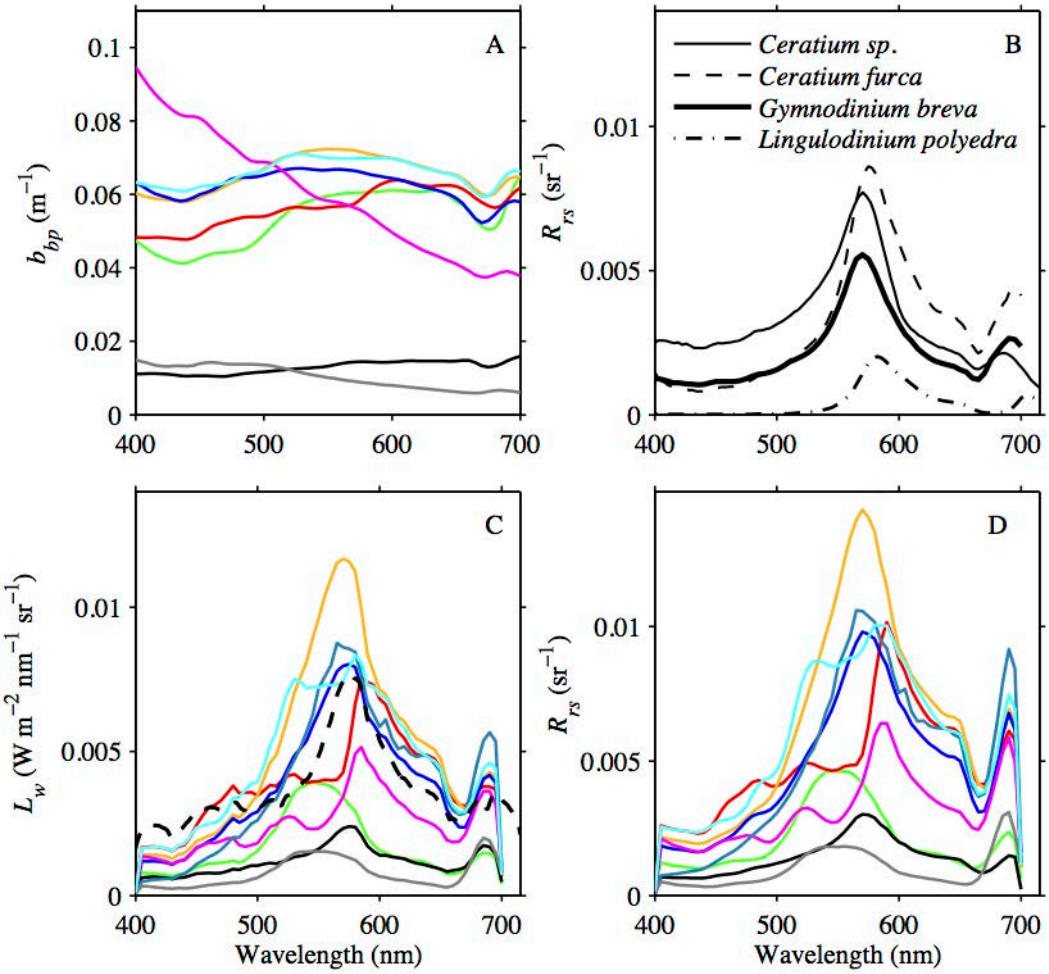

Fig. 2. (A) Backscattering estimated for phytoplankton concentrations of 30 mg Chl *a* m^{-3} for each taxon (Stramski et al. 2001), as defined in Fig. 1. (B) Remote sensing reflectance, R_{rs}, measured from a variety of dinoflagellate red tides along the California coast. *Lingulodinium polyedra* spectrum provided courtesy of G. Chang. (C) Water-leaving radiance, L_w, modeled for dense phytoplankton bloom conditions (30 mg Chl *a* m^{-3}) from a variety of phytoplankton taxa. (D) Data from panel (C) shown as R_{rs}.

The role of backscattering—The quantity and spectral quality of light reflected from the sea surface is not related just to the unabsorbed photons in the water column, but is also proportional to the amount of photons that are scattered in the backward direction out of the water column (i.e., backscattering). The reflectance of light at the sea surface (R) is governed by the ratio of backscattering (b_b) to absorption (a) (Gordon and Morel 1983), such that

$$R \propto \frac{b_b}{a + b_b} \tag{7}$$

The amount and type of suspended materials (e.g., phytoplankton, sediment, minerals, etc.) will determine the magnitude and spectral shape of particulate backscattering (Stramski and Kiefer 1991). Backscattering properties of phytoplankton can vary with cell size, growth rate, and species composition. The phytoplankton taxa considered here have backscattering properties that vary spectrally (Stramski et al. 2001). As shown in Fig. 2A, small phytoplankton, like *Synechococcus* and *Prochlorococcus*, have enhanced backscattering of blue photons and the spectral shape is negatively sloping. Larger phytoplankton have backscattering spectra that are nearly constant with wavelength or positively sloping (higher in the red). Our simulations used chlorophyll-normalized particulate backscattering coefficients (b_p^*), such that particulate backscattering increased linearly with increasing Chl *a*. This has been shown both theoretically (Morel 1988; Stramski and Kiefer 1991) and experimentally from a large database of in situ backscattering measurements with Chl *a* concentrations ranging over 100 mg m^{-3} (Sullivan et al. 2005).

In order for the sea surface to appear red, more red light must be backscattered out of the water than other colors of light. The definition of red light is generally considered to be light at wavelengths greater than 600 nm. Hyperspectral reflectance measurements made of the sea surface during red tides, however, typically show maximum spectral reflectance at wavelengths less than 600 nm (Fig. 2B; Carder and Steward 1985). Similar spectra are also derived from our modeling efforts (Fig. 2C,D). For many of the phytoplankton taxa considered, including the diatoms and dinoflagellates, our simulations showed a maximum spec-

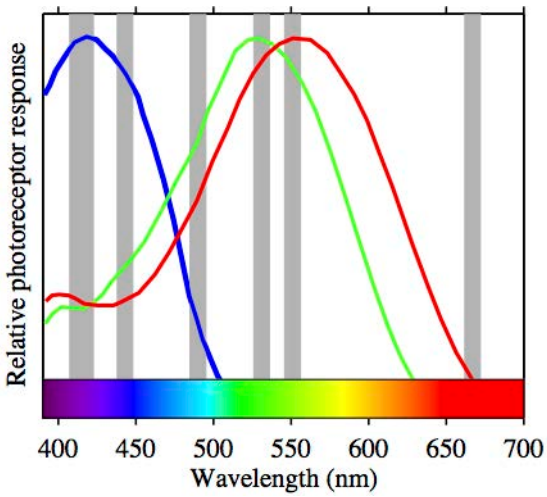

Fig. 3. Response of the three cone classes (short, middle, and long) in the human eye to different wavelengths of light (scaled to the same range, Livingstone 2002). The bottom color spectrum indicates the color associated with individual wavelengths of light. The gray bars represent the wavelengths used by the Moderate Resolution Imaging Spectroradiometer (MODIS) ocean color sensor.

tral peak in both reflectance and water-leaving radiance at 570–580 nm, a region of the visible spectrum usually characterized as yellow light (Fig. 2C,D). The width and peak of the R_{rs} and L_w spectra, however, do vary by taxa. The spectral peak in reflectance for both Rhodophyceae and *Synechococcus* are shifted further into the red near 600 nm, while the spectrum for Chlorophyceae is less peaked and centered at 550 nm. A lesser peak in reflectance caused by solar-stimulated chlorophyll fluorescence is visible at 683 nm (Smith and Baker 1978), but this peak is generally lower in magnitude than the primary peak and not influential to the color perceived by the human eye (*see following*). Extremely dense algal blooms (>100 mg Chl *a* m^{-3}) can peak at or beyond 600 nm (Roesler and Boss 2003), but this is not required for the water to appear red. Color perception, however, involves more than just the peak spectral reflectance and requires consideration of the entire spectrum of light relative to receptors within the human eye.

The role of human color vision—Understanding the perception of sea surface color requires a consideration of the physiological characteristics of the human eye. Human vision involves three different cone receptors and a fourth type of photoreceptor cell referred to as a rod. Rods are effective only in low light levels (referred to as night vision) and are not important for interpreting sea surface color. The three cone receptors in the eye, referred to as long-, middle-, and short-wavelength cones, are responsible for our color vision (Fig. 3). Each cone contains unique pigments that respond to a different range of visible wavelengths (Williamson and Cummins 1983). These cones are sometimes called red, green, and blue cones, although the red wavelength cone response is actually centered in the yellow region of the visible spectrum. The red cone pigment evolved 30–40 million years ago by a minor mutation in the green cone pigment that shifted the absorption peak about 30 nm to the red and is absent in individuals who are red/green colorblind (Livingstone 2002). The color perceived by the human visual system depends on the total light or radiance incident upon each type of cone and the comparative response (i.e., contrast) between the three cone classes.

When phytoplankton become densely concentrated at the sea surface, blue/blue-green light is absorbed proportionally to the amount of Chl *a* (Fig. 4A), and the reflected light or water-leaving radiance incrementally shifts to longer wavelengths (Fig. 4B). Absorption by water rises steeply beyond 570 nm (Smith and Baker 1981; Pope and Fry 1997) and results in a maximum L_w peak between 570 and 600 nm. In addition, increasing phytoplankton concentrations typically result in increased L_w from 550 to 700 nm due to enhanced backscattering (Fig. 4B). When normalized to the peak radiance (Fig. 4C), changes in the shape of the radiance spectra are evident with increasing Chl *a*. The radiance distribution appears relatively similar in peak width as Chl *a* increases from 10 to 50 mg m^{-3}, but the entire spectrum swings like a bell toward the red as more blue light is absorbed and more red light is backscattered.

Perceived color was modeled from water-leaving radiance spectra using an empirically derived color coordinate system (CIE 1991). When the color is a red hue, the total light absorbed by the eye's red cones is greater than that absorbed by the green and blue cones. Brown coloration can be considered a dull red and occurs when all three cones are stimulated, but with the greatest activation of the red cones. We modeled water-leaving radiance as a function of average absorption and backscattering properties for increasing concentrations of different phytoplankton taxa concentrated at the sea surface. As phytoplankton concentrations increased, more blue/green light was absorbed and more red light was backscattered out of the water. Perceived color progressed from blue, to green, and finally to red or red/brown for the majority of phytoplankton taxa (Fig. 5A). These results are also represented on a chromaticity diagram (Kelly 1943) for three representative taxa: Chlorophyceae, Bacillariophyceae, and Rhodophyceae (Fig. 5B). The *x, y* coordinates represent the fraction of the spectra intercepted by the red and green cones, respectively, and the residual from unity is the fraction intercepted by the blue cones (*z*). For example, light at 520 nm is represented by 10% red (*x*), 80% green (*y*), and by derivation 10% blue (*z*). Of the phytoplankton considered, only *Prochlorococcus* and certain species of Chlorophyceae (*Cunaliella bioculata*) did not produce red or brown coloration at high concentrations.

At a modeled threshold concentration near 15 mg Chl *a* m^{-3} for most phytoplankton taxa, the eye's red cones (centered at 564 nm) are activated more than the green cones (centered at 534 nm) and the water appears reddish brown. This shift in color is not due to any special absorption or backscattering properties of the algae but is due to the human visual system. The peak in the water-leaving radiance spectra from dense algal blooms coincides with a critical visual hinge point where the green and red

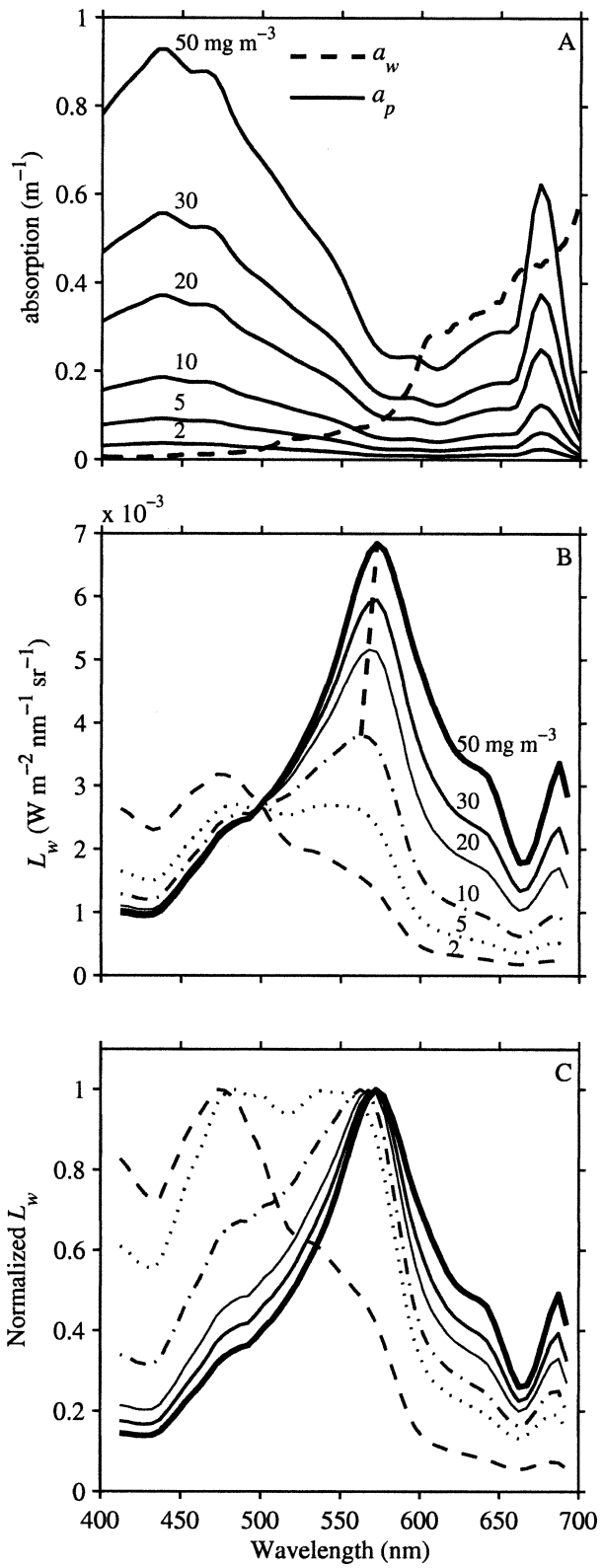

Fig. 4. (A) Particulate absorption coefficient for a diatom showing the increase in absorption with increasing concentration. The wavelength at which absorption due to phytoplankton and that due to pure water (Pope and Fry 1997) intersect represents the minimum in absorption and the maximum or peak reflectance. (B) Spectral variability in water-leaving radiance (L_w) modeled for a diatom bloom with increasing Chl *a* concentrations (2, 5, 10, 15, 20, 30, 40, 50 mg m^{-3}). Dotted line shows the peak wavelengths. (C) Spectra from panel (B) normalized to peak water-leaving radiance. The corresponding color associated with each spectrum is shown in the results for Bacillariophyceae in Fig. 5A.

cones are nearly equally stimulated (570 nm). Subtle spectral changes in L_w about this critical hinge point produce large shifts in the observed color from green to red.

Sensitivity analysis—To address uncertainties in our modeling assumptions, we conducted a sensitivity analysis varying the particulate backscattering and absorption properties of the water, as well as the incident light field. These simulations used the total upward radiance from the sea surface (L_u), which includes water-leaving radiance (L_w) plus the downwelling irradiance reflected off the sea surface. The simulations for scenario 1 used a fixed absorption coefficient (Dinophyceae) at 30 mg m^{-3} (Fig. 6A) and variable particulate backscattering ratios ranging from 0.6% to 2% (Fig. 6B). The resulting L_u was characterized by a distinct peak at 570 nm regardless of the backscattering spectrum used in the model (Fig. 6C). This is because peak reflectance is largely determined by the combined absorption properties of pure water and phytoplankton. In addition, L_u spectra increase monotonically with increasing backscattering (Fig. 6C). When normalized to peak L_u, however, all cases had nearly identical spectral shapes resulting in a similar greenish-brown color (Fig. 6D). Changes in the magnitude of backscattering, without corresponding changes to the spectral shape of backscattering, will alter the perceived brightness or luminance of the water, but these changes have little impact on the color.

In scenario 2, three different backscattering spectra were used to illustrate how subtle variations in the radiance spectra about the 570 nm hinge point produce large changes in the perceived color of the sea surface (Fig. 6E–H). As shown in Fig. 6F, backscattering spectral shapes varied from (1) negatively sloped backscattering (greater in the blue than the red), (2) spectrally flat backscattering, and (3) positively sloped backscattering (greater in the red than the blue). The positively sloped simulation had the highest backscattering from 500 to 700 nm and resulted in the largest L_u peak (Fig. 6G). The three cases also produced significant differences in the spectral shape of L_u that resulted in widely differing colors. Even though the peak reflectance was the same for all cases, negatively sloped backscattering enhanced the blue reflectance and resulted in a greenish hue. In contrast, positively sloped backscattering enhanced red reflectance and resulted in a reddish-brown hue.

These results were not duplicated, however, in scenario 3 where green algae (Chlorophyceae) were the predominant phytoplankton (Fig. 6I–L). Lacking sufficient green-absorbing accessory pigments (Fig. 6I), these phytoplankton produced a broad and rounder radiance peak spanning the entire 500–600 nm region. Distinct spectral shapes were

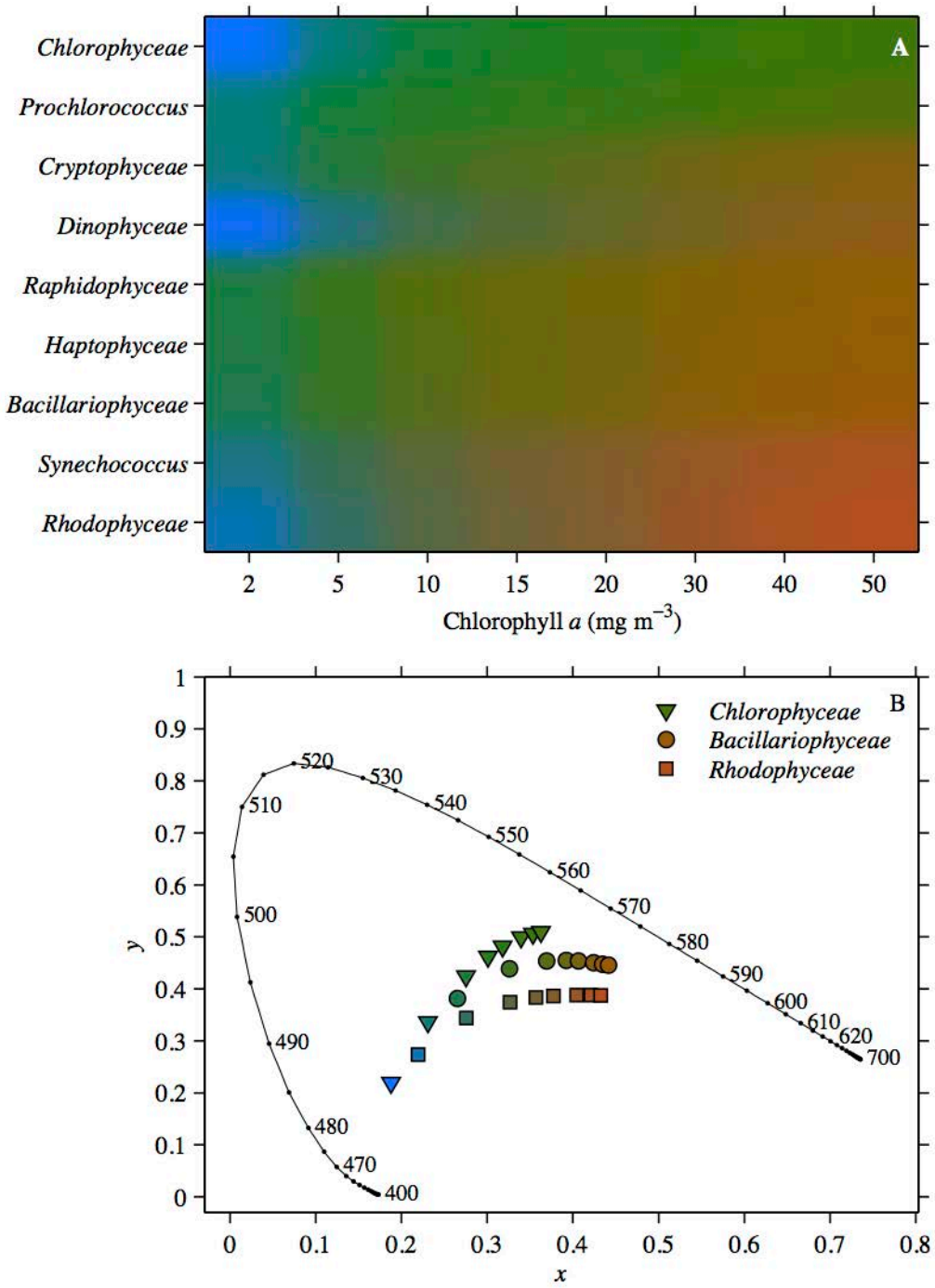

Fig. 5. (A) Color of the sea surface as a function of surface biomass concentration (Chl *a* used as a proxy) for different phytoplankton taxa. Color was modeled from water-leaving radiance using the CIE color matching functions and mean absorption and backscattering properties for each taxa. (B) The chromaticity coordinates for a selection of three algal taxa are shown on a CIE chromaticity diagram (Kelly 1943) as Chl *a* increases from 2 mg m^{-3} (lower left points) to 50 mg m^{-3} (upper right points). For clarity, the color of each symbol corresponds to the color presented for that algal group in panel (A).

observed with the different backscattering shapes, but the resulting sea surface color was a similar shade of green for all simulations (Fig. 6L).

Scenario 4 explored variations in the incoming downwelling irradiance field on perceived water color (Fig. 6M–P). The simulations covered a range of solar zenith angles (SZA) from nearly overhead (10°) to nearly at the horizon (80°). The highest L_u occurred when the sun was nearly overhead (SZA 10°) because of the greater amount of light reaching the sea surface (Fig. 6O; note axis is four times

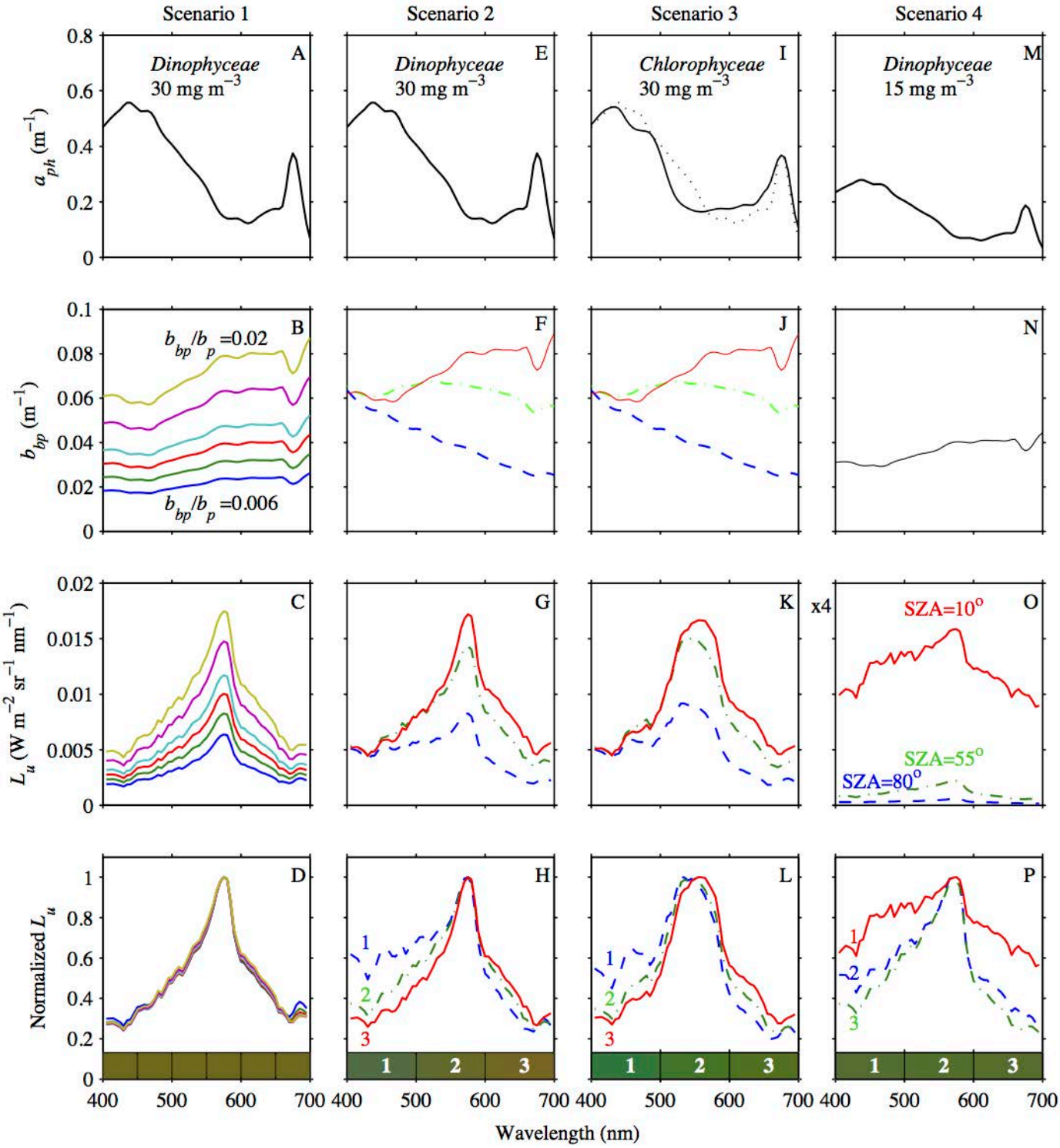

Fig. 6. Sensitivity analysis of particulate absorption, backscattering, and solar zenith angle (SZA) on modeled upwelling radiance at the sea surface and resulting color. Each column represents a different modeling scenario (1–4) used in the hydrolight radiative transfer model (Mobley 1994). The first row of panels provides the phytoplankton absorption properties, a_{ph}, for each scenario. The second row provides the particulate backscattering, b_{bp}. The upwelling radiance spectra, L_u, modeled at the sea surface using the absorption and backscattering properties is shown in the third row of panels. Note that the scale for panel O is four times that of panels C, G, and K. The fourth row is the L_u spectra normalized to the peak L_u and represents the relative contributions of radiance in each wavelength. The bottom color bars show the resulting colors modeled from each spectrum.

higher than the other plots). When normalized to peak radiance, the case with 10° SZA showed elevated radiance across the whole spectrum (both the blue and red wavelengths). This is largely due to reflected skylight, which represents photons that are scattered by the sea surface without penetrating the water column. The resulting spectral whitening produced more luminance but did not significantly change the perceived color of the water (Fig. 6P).

Thus, the production of reddish water requires phytoplankton with sufficient accessory pigments to shift the radiance spectrum toward the critical visual hinge point (570 nm). Simply amplifying the amount of backscattering, without changing the spectral backscattering shape or simultaneously increasing absorption, does not change the spectral shape of L_u or the resulting color of the water. Phytoplankton with higher backscattering in the red produce brown/red–colored water at lower overall phytoplankton concentrations than those that backscatter more blue photons. A low sun angle can produce a more luminous spectrum because of reflected photons but is not responsible for brown/red–colored water. In general, algal absorption properties determine whether dense concentrations of a particular phytoplankton group can potentially cause red-colored water, but taxon-specific backscattering properties can influence the amount of phytoplankton necessary to produce red coloration.

Fluorescence and the red edge—Measured reflectance spectra from a variety of dinoflagellate red tides show a prominent secondary peak in the far-red region of the spectrum (Fig. 2A). At first glance, these peaks appear to be associated with chlorophyll fluorescence, an important pathway for the dissipation of light energy (Smith and Baker 1978). However, the peak wavelengths are not always centered at the chlorophyll fluorescence peak of 683 nm but can be shifted further into the near infrared (NIR) (>700 nm). For example, the reflectance spectrum from the dinoflagellate *L. polyedra* (Fig. 2A) has a peak at 710 nm. This is not from fluorescence alone, but appears to be caused by what the terrestrial remote sensing community calls the red edge.

Terrestrial vegetation and submerged macrophytes (sea grasses and seaweeds) exhibit strong reflectance in the NIR portion of the spectrum (700–1,600 nm, Hall 1994). This NIR reflectance is commonly attributed to scattering from cell and leaf structures (cell walls and membranes, organelles, air spaces, etc.) and forms the basis of the terrestrial biomass parameter normalized difference vegetation index (NDVI, Hall 1994). However, plant cell structures are capable of scattering visible, as well as NIR, radiation. In fact, reflectance from unpigmented white leaves lacks a red edge because light is reflected similarly across both the visible and NIR portions of the spectrum (Gitelson and Merzlyak 1994; Zimmerman unpubl. data). Thus, photosynthetic pigments produce the red edge signature by absorbing visible, but not NIR, radiation. NIR reflectance is generally ignored for dilute suspensions of microscopic phytoplankton because water strongly absorbs these photons. For most natural populations of phytoplankton, the peak reflectance observed in the far-red region can be assigned to fluorescence. However, pigmented microalgae also reflect NIR light with much higher efficiency than visible light (Fig. 7). For dense suspensions of algal cells at the sea surface (i.e., red tides), the infrared reflectance signal can be strong enough that it is not fully attenuated by the water, producing peaks in the reflectance spectra that are red-shifted relative to those produced by chlorophyll fluorescence (Vasilkov and Kopelevich 1982; Gitelson 1992).

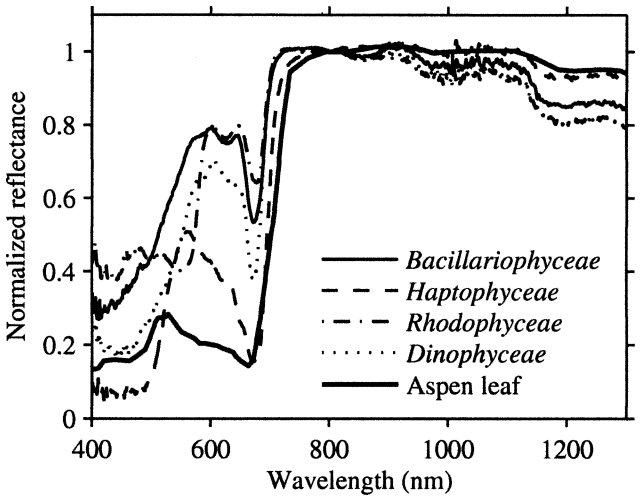

Fig. 7. Relative reflectance of unicellular algal cultures captured onto GF/F filters increases strongly from 680 to 710 nm, producing a red edge typical of photosynthetic tissues. The reflectance spectrum from a terrestrial aspen leaf (Hall et al. 1991) is shown for comparison. Spectra are normalized to reflectance at 800 nm and do not contain a solar-stimulated fluorescence peak centered at 683 nm.

While it is an important feature of red tide spectra, enhanced reflectance due to fluorescence and the red edge has little impact on the perceived color of the sea surface. The response of the human red cone, which is tuned to 564 nm, is very low at wavelengths greater than 650 nm (Fig. 3). Light at longer red wavelengths can be perceived when it originates from a concentrated source (i.e., a laser), but the low levels produced by chlorophyll fluorescence or red edge reflectance are simply not perceptible under most natural light conditions. Thus, the perceived sea surface color modeled for different phytoplankton (Fig. 5) did not change when reflectance greater than 650 nm was excluded from the analysis and is largely independent of chlorophyll fluorescence and the red edge. Enhanced radiance in the NIR is not important for color vision but has significant implications for understanding algal backscattering, for understanding atmospheric correction of remotely sensed imagery, and for developing new methods for remote sensing of red tides.

Red and black tides caused by CDOM and sediments—Our modeling indicates that optical properties of many different phytoplankton taxa can produce red coloration if cells are sufficiently concentrated at the sea surface. A red

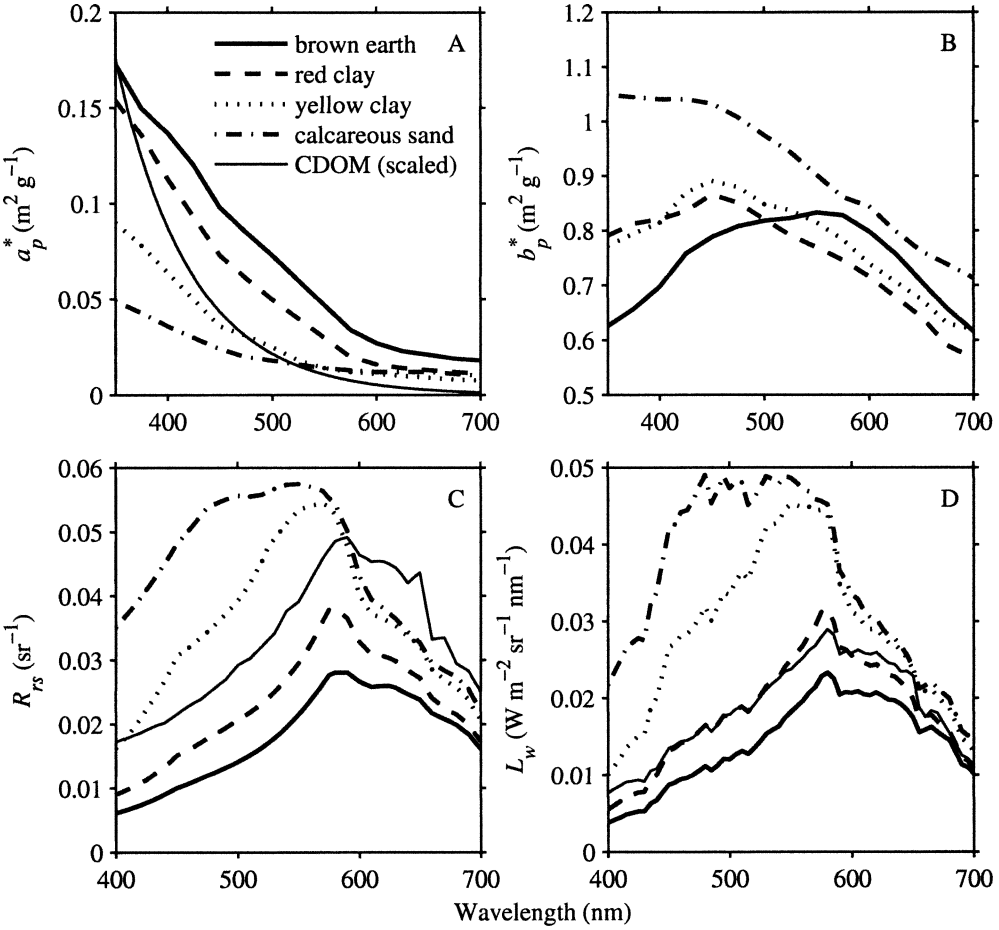

Fig. 8. (A) Mass-specific particulate absorption coefficients and (B) scattering coefficients for various mineral types (Ahn 1990). (C) Remote sensing reflectance spectra, R_{rs}, and (D) water-leaving radiance spectra, L_w, modeled using the optical properties for a mineral concentration of 20 g m^{-3}. Absorption and reflectance spectra for waters dominated by colored dissolved organic matter (CDOM) are shown for comparison (scaled to fit).

coloration can also result from nearly any constituent that is a blue/green absorber provided enough light is back-scattered out of the water column. CDOM is a common component of coastal water that absorbs light in the blue region of the spectrum (Fig. 8A; Kirk 1976). The CDOM absorption spectrum decreases exponentially from blue to red. Suspended sediments also absorb light predominantly in the blue region of the spectrum (Fig. 8A), but the spectral shape depends on the suite of minerals present (Morel and Prieur 1977; Ahn 1990; Babin and Stramski 2004). Unlike CDOM, minerals have a large refractive index and high backscattering coefficients (Fig. 8B). Minerals suspended in water can produce reflectance spectra that are several orders of magnitude greater than water with CDOM, or even phytoplankton, alone. As originally noted by Morel and Prieur (1977) in their early delineation of Case 2 waters, waters dominated by sediments and CDOM have flatter and broader reflectance spectra from 600 to 650 nm (Fig. 8C,D) compared to water with dense phytoplankton concentrations. This is because the absorption coefficient for these constituents monotonically decreases with increasing wavelength, unlike phytoplankton pigments, which absorb both blue and red light.

Here, we modeled sea surface color as a function of increasing CDOM and suspended sediments or minerals (Fig. 9). Because CDOM does not scatter light, waters that are highly concentrated in CDOM alone are so dark that they appear black in color (Acker and Kempler 2004; Fig. 9A). An example of a black river that has high CDOM concentrations can be found in the Rio Negro, Brazil (Fig. 9C). Black water can also occur during intense phytoplankton blooms that have low backscattering (Carder and Steward 1985; Hu et al. 2004). High concentrations of CDOM will produce a red/brown coloration of the sea surface, however, when suspended materials that can scatter light out of the water column are also present in the water. Optically shallow water systems with a highly reflective bottom can also appear red/brown in the presence of high CDOM concentrations (Fig. 9D). Such high CDOM concentrations are seldom observed in the open ocean but are most likely to be found in estuarine waters where the terrestrial sources of CDOM are greatest (Kirk 1976; Twardowski et al. 2004).

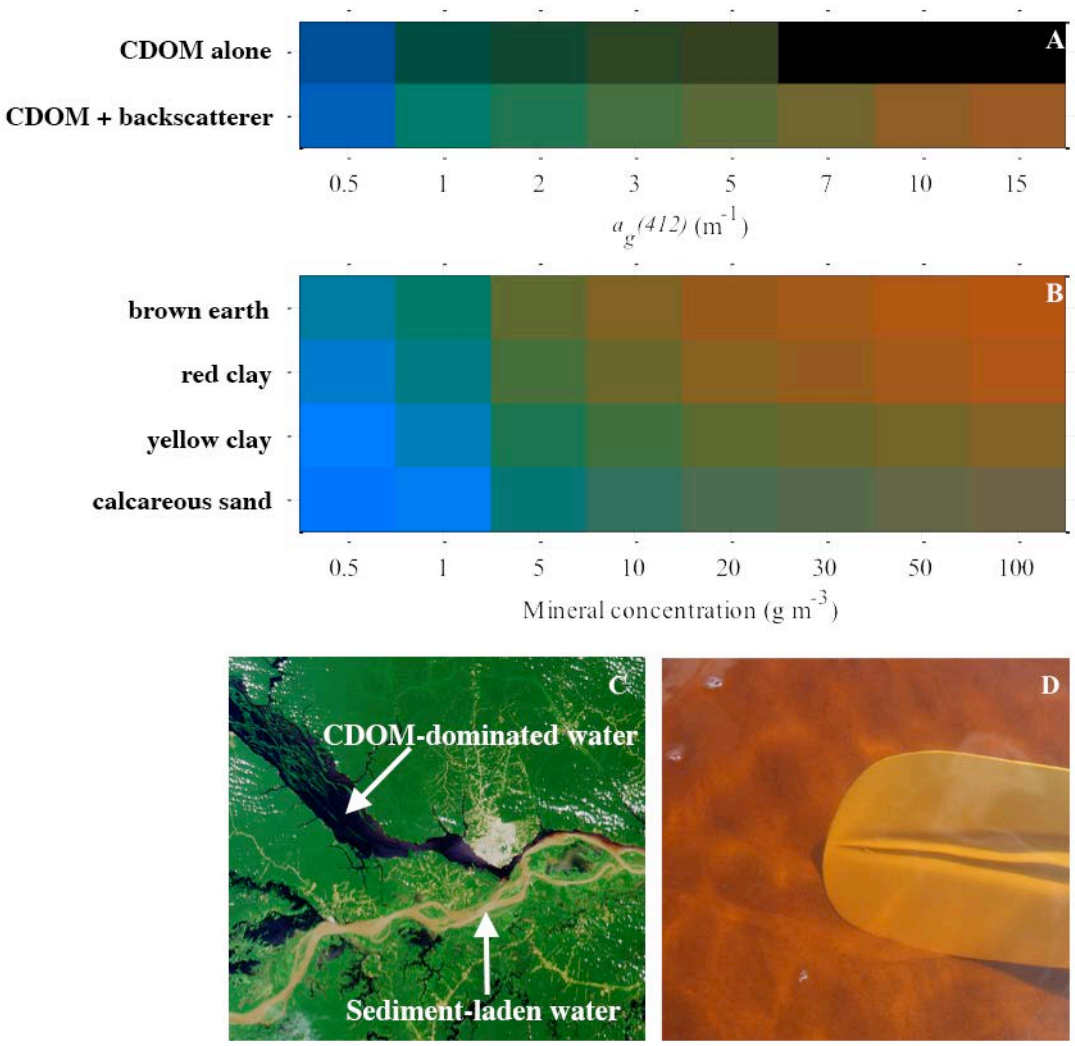

Fig. 9. Color of the sea surface as a function of increasing concentrations of (A) colored dissolved organic matter (CDOM), shown as absorption at 412 nm, and CDOM with the addition of nonabsorbing backscattering matter, and (B) four different types of minerals. (C) Satellite image of the confluence of the black waters of the Rio Negro in the north and the sediment-laden Rio Solimoes to the southeast in Manuas, Brazil. Multi-angle imaging spectroradiometer (MISR) image obtained from the NASA Goddard Earth Sciences Data and Information Services Center Web site (Acker and Kempler 2004). (D) Photo showing the water color of a shallow inlet in Western Australia containing high CDOM concentrations (courtesy of G. Chang). White kayak paddle is shown for perspective.

Waters with high mineral content (>10–15 g m^{-3}) also produced red or brown colored water (Fig. 9B). From the limited set of minerals considered here, brown earth and red clay have the greatest absorption coefficient per mass and created red-colored water. Yellow clay and calcareous sand absorbed less of the blue/green light and produced a brownish hue when concentrated. Mineral particles with significant amounts of iron absorb more of the blue-green light (Babin and Stramski 2004) and would create even redder coloration at lower concentrations.

Remote detection of red tides—The radiance spectra modeled for water dominated by surface layers of different phytoplankton, CDOM, and minerals have unique spectral signatures that may allow us to discriminate these constituents remotely from satellites or aircraft. As shown in Fig. 2C, high concentrations of cryptophytes can result in a double peaked reflectance spectrum. Dense concentrations of red algae produce an asymmetric spectral peak that is shifted toward the red region of the spectrum. Green algae are distinguished by a broad spectral maximum centered at 540 nm. Unfortunately, the two most common red tide–forming phytoplankton in the coastal ocean, dinoflagellates and diatoms (Sournia 1995), have similar absorption characteristics and will be the most difficult to differentiate based solely on optical signatures (Schofield et al. 1999; Roesler et al. 2003). Waters dominated by CDOM

and sediments produce broader reflectance spectra compared to phytoplankton-dominated waters.

Current space-borne ocean color sensors can view dense algal blooms (Kahru et al. 2004) and sediment plumes but have limited spectral capabilities. These sensors provide no information in the region of the spectrum where red tides peak and where most of the taxon-specific differences occur in water-leaving radiance (570–610 nm). Several airborne hyperspectral sensors can provide the spectral information needed to detect taxon-specific differences from ocean color (Chang et al. 2004; Ryan et al. 2005), and their use will be critical for monitoring red tide formation and remotely detecting phytoplankton composition in many coastal regions. Enhanced reflectance in the NIR due to fluorescence and the red edge may also be critical for remotely detecting surface blooms of algae.

Understanding the nuances of the color produced by increasing concentrations of different groups of algae or other water column constituents across the whole visible and NIR spectrum can lead to better remote monitoring and forecasting of dense algal blooms that may have harmful consequences. By combining hyperspectral imagery with a variety of monitoring platforms and parameters, it may be possible to develop probabilistic models of toxic algal blooms, or ecological algorithms (Schofield et al. 1999; Stumpf et al. 2003; Etheridge and Roesler 2004; Babin et al. 2005; Kudela et al. 2005). Future research may allow us to predict the probability of harmful algal bloom development, monitor the extent and longevity of the bloom, and forecast the coastal region to be affected by the bloom. Our research shows that the visual identification of red water is strongly affected by human physiology, in addition to the absorbing and scattering components of natural waters. Moreover, the presence of red water does not necessarily indicate a dense or harmful algal bloom, but can result from various combinations of phytoplankton, CDOM, and minerals.

References

Acker, J., and S. Kempler. 2004. Oh black waters, keep on rollin'. *Science Focus* [Internet]. Washington (DC): National Aeronautics and Space Administration, Available from http://daac.gsfc.nasa.gov/oceancolor/scifocus/oceanColor/black_water.shtml. Accessed 1 May 2005.

Ahn, Y. H. 1990. Optical properties of biogenous and numerical particles in the ocean; application: Inversion of reflectance. Ph.D. thesis, Univ. Pierre et Marie Curie. QC/425/YB/1990 [in French].

Anderson, D. M. 1994. Red tides. Sci. Am. **271:** 52–58.

Arnone, R. A., A. M. Wood, and R. W. Gould. 2004. The evolution of optical water mass classification. Oceanography **17:** 14–15.

Babin, M., and D. Stramski. 2004. Variations in the mass-specific absorption coefficient of mineral particles in sea water. Limnol. Oceanogr. **49:** 756–767.

———, and others. 2005. New approaches and technologies for observing harmful algal blooms. Oceanography **18:** 210–227.

Balch, W. M., and K. A. Kilpatrick. 1992. Particulate reflectance measurements of phytoplankton. J. Plankton Res. **14:** 721–735.

The Bible. Exodus **7:** 20–21.

Bricaud, A., M. Babin, A. Morel, and H. Claustre. 1995. Variability in the chlorophyll-specific absorption coefficients of natural phytoplankton: Analysis and parameterization. J. Geophys. Res. **100:** 13,321–13,332.

Carder, K. L., and R. G. Steward. 1985. A remote-sensing reflectance model of a red-tide dinoflagellate off west Florida. Limnol. Oceanogr. **30:** 286–298.

Chang, G., and others. 2004. The new age of hyperspectral oceanography. Oceanography **17:** 16–23.

[CIE] Commission Internationale de l'Êclairage. 1991. Colorimetric observers. ISO/CIE 10527.

Ciotti, A. M., J. J. Cullen, and M. R. Lewis. 2002. Assessment of the relationships between dominant cell size in natural phytoplankton communities and the spectral shape of the absorption coefficient. Limnol. Oceanogr. **47:** 404–417.

Cleveland, J. S., and A. D. W. Weidemann. 1993. Quantifying absorption by aquatic particles: A multiple scattering correction for glass-fiber filters. Limnol. Oceanogr. **38:** 1321–1327.

Cullen, J. J., A. M. Ciotti, R. F. Davis, and M. R. Lewis. 1997. Optical detection and assessment of algal blooms. Limnol. Oceanogr. **42:** 1223–1239.

Dierssen, H. M. 2006. MATLAB code for determining RGB colors from a radiance spectrum. Available from http://colors.uconn.edu/.

Encyclopedia Britannica. 2004. Red tide [Internet]. Encyclopedia Britannica [accessed 2004 September 10]. Available from http://www.britannica.com/eb/article?tocId=9376627.

Etheridge, S., and C. S. Roesler. 2004. Temporal variations in phytoplankton, particulate, and colored dissolved organic material based on optical properties during a Long Island brown tide compared to an adjacent embayment. Harmful Algae **3:** 331–342.

Fournier, G. R., and J. L. Forand. 1994. Analytic phase function for ocean water. Ocean Optics VII. Proceedings of the International Society for Optical Engineering (SPIE) **2258:** 194–201.

Gitelson, A. 1992. The peak near 700 nm on radiance spectra of algae and water: Relationships of its magnitude and position with chlorophyll concentration. Int. J. Remote Sens. **13:** 3367–3373.

———, and M. N. Merzlyak. 1994. Spectral reflectance changes associated with Autumn senescence of *Aesculus hippocastanum* L. and *Acer platanoides* L. leaves. J. Plant Physiol. **143:** 286–292.

Glibert, P. M., D. M. Anderson, P. Gentien, E. Graneli, and K. G. Sellner. 2005. The global, complex phenomena of harmful algal blooms. Oceanography **18:** 136–147.

Gordon, H. R., and A. Y. Morel. 1983. Remote assessment of ocean color for interpretation of satellite visible imagery: A review. Springer-Verlag.

Hall, F. G. 1994. Adaptation of NASA remote sensing technology for regional-level analysis of forested ecosystems. *In* V. A. Sample [ed.], Remote sensing and GIS in ecosystem management. Island Press..

———, D. B. Botkin, D. E. Strebel, K. D. Woods, and S. J. Goetz. 1991. Large-scale patterns of forest succession as determined by remote sensing. Ecology **72:** 628–640.

Hallegraeff, G. M. 2003. *In* G. M. Hallegraeff, D. M. Anderson, and A. D. Cembella [eds.], Manual on harmful marine microalgae. UNESCO..

Harding, L. W. 1998. The time-course of photoadaptation to low-light in *Prorocentrum mariae lebouriae* (Dinophyceae). J. Phycol. **24:** 274–281.

Hu, C., F. E. Muller-Karger, G. A. Vargo, M. B. Neely, and E. Johns. 2004. Linkages between coastal runoff and the Florida Keys ecosystem: A study of a dark plume event. Geophys. Res. Lett. **31**, L15307. [doi: 10.1029/2004GL020382].

Hutchinson, G. E. 1975. A treatise on limnology. Geography and physics of lakes. Wiley.

[ITU-R] International Telecommunication Union—Radiocommunication. 2002. Parameter values for the HDTV* standards for production and international programme exchange, Rec. BT. 709-5. ITU-R.

Kahru, M., B. G. Mitchell, A. Diaz, and M. Miura. 2004. MODIS detects a devastating algal bloom in Paracas Bay, Peru. EOS Trans. Am. Geophys. Union **85:** 465–472.

Kelly, K. L. 1943. Color designation for lights. J. Opt. Soc. Am. **33:** 627–632.

Kirk, J. T. O. 1976. Yellow substance (gelbstoff) and its contribution to the attenuation of photosynthetically active radiation in some inland and coastal southeastern Australian waters. Aus. J. Mar. Freshw. Res. **27:** 61–71.

———. 1994. Light and photosynthesis in aquatic ecosystems, 2nd ed. Cambridge Univ. Press.

Kudela, R. M., G. Pitcher, T. Probyn, F. Figuerias, T. Moita, and V. Trainer. 2005. Harmful algal blooms in coastal upwelling systems. Oceanography **18:** 184–197.

Livingstone, M. 2002. Vision and art: The biology of seeing. Harry N. Abrams.

Millie, D. F., O. Schofield, G. J. Kirkpatrick, G. Johnsen, P. Tester, and B. Vinyard. 1997. Detection of harmful algal blooms using photopigments and absorption signatures: A case study of the Florida red-tide dinoflagellate, *Gymnodinium breve*. Limnol. Oceanogr. **42:** 1240–1251.

Mobley, C. D. 1994. Light and water: Radiative transfer in natural waters. Academic.

———. 1999. Estimation of the remote sensing reflectance from above-surface measurements. Appl. Opt. **38:** 7442–7455.

Morel, A. 1988. Optical modeling of the upper ocean in relation to its biogenous matter content (Case I waters). J. Geophys. Res. **93:** 10,749–10,768.

———, and L. Prieur. 1977. Analysis of variations in ocean color. Limnol. Oceanogr. **22:** 709–722.

Pope, R., and E. Fry. 1997. Absorption spectrum of pure water: 2. Integrating cavity measurements. Appl. Opt. **36:** 8710–8723.

Roesler, C. S., and E. Boss. 2003. Spectral beam attenuation coefficient retrieved from ocean color inversion. Geophys. Res. Lett. **30**, 1468 [doi: 10.1029/2002GL016185].

———, S. M. Etheridge, and G. C. Pitcher. 2003. Application of an ocean color algal taxa detection model to red tides in the Southern Benguela. *In* K. A. Steidinger, J. H. Lansdberg, C. R. Toma and G. A. Vargo [eds.], Proceedings of the Xth International Conference on Harmful Algae. Florida Fish and Wildlife Conservation Commission and Intergovernmental Oceanographic Commission of UNESCO.

Ryan, J., and others. 2005. Coastal ocean physics and red tides: An example from Monterey Bay, California. Oceanography **18:** 246–255.

Sathyendranath, S., L. Lazzara, and L. Prieur. 1987. Variations in the spectral values of specific absorption of phytoplankton. Limnol. Oceanogr. **32:** 403–415.

Schofield, O., J. Gryzmski, W. P. Bissett, G. J. Kirkpatrick, D. F. Millie, M. Moline, and C. S. Roesler. 1999. Optical monitoring and forecasting systems for harmful algal blooms: Possibility or pipe dream? J. Phycol. **35:** 1477–1496.

Smith, R. C., and K. S. Baker. 1978. Optical classification of natural waters. Limnol. Oceanogr. **23:** 260–267.

———, and ———. 1981. Optical properties of the clearest natural waters. Appl. Opt. **20:** 177–184.

———, ———, and P. Dustan. 1981. Fluorometric techniques for the measurement of oceanic chlorophyll in the support of remote sensing. SIO Ref. 81–17. Visibility Laboratory, Scripps Institution of Oceanography, Univ. of California, San Diego.

Sournia, A. 1995. Red-tide and toxic marine phytoplankton of the world ocean: An inquiry into biodiversity, p. 103–112. *In* Harmful Algal Blooms, Proceedings of the Sixth International Conference on Toxic Marine Phytoplankton, October 1993, Nantes, France. Lavoisier.

Stramski, D., A. Bricaud, and A. Morel. 2001. Modeling the inherent optical properties of the ocean based on the detailed composition of the planktonic community. Appl. Opt. **40:** 2929–2945.

———, and D. A. Kiefer. 1991. Light scattering by microorganisms in the open ocean. Prog. Oceanogr. **28:** 343–393.

Stumpf, R. P., and others. 2003. Monitoring *Karenia brevis* blooms in the Gulf of Mexico using satellite ocean color imagery and other data. Harmful Algae **2:** 147–160.

Sullivan, J. M., M. S. Twardowski, P. L. Donaghay, and S. A. Freeman. 2005. Use of optical scattering to discriminate particle types in coastal waters. Appl. Opt. **44:** 1667–1680.

Tassan, S., and G. M. Ferrari. 1995. An alternative approach to absorption measurements of aquatic particles retained on filters. Limnol. Oceanogr. **40:** 1358–1368.

Twardowski, M. S., E. Boss, J. B. Macdonald, W. S. Pegau, A. H. Barnard, and J. R. V. Zaneveld. 2001. A model for estimating bulk refractive index from the optical backscattering ratio and the implications for understanding particle composition in case I and case II waters. J. Geophys. Res. **105:** 14,129–14,142.

———, ———, J. M. Sullivan, and P. L. Donaghay. 2004. Modeling the spectral shape of absorption by chromophoric dissolved organic matter. Mar. Chem. **89:** 69–88.

Ulloa, O., S. Sathyendranath, and T. Platt. 1994. Effect of the particle-size distribution on the backscattering ratio in seawater. Appl. Opt. **33:** 7070–7077.

Vasilkov, A., and O. Kopelevich. 1982. The reasons of maximum at about 700 nm on radiance spectra of the sea. Oceanology **22:** 945–950.

Williamson, S. J., and H. Z. Cummins. 1983. Light and color in nature and art. Wiley.

Yoder, J. A. 2000. Terra's view of the sea. Science **288:** 1978–1980.

Received: 16 August 2005
Accepted: 10 May 2006
Amended: 12 June 2006